Research Article

Nadine Bauer, Frank van den Boom, Nico Marx, Karin B. Busch, Gerhard Holst and Friedemann Kiefer*

Live-cell FLIM of a genetically encoded reporter reveals oxygen equilibration in cultured cells

https://doi.org/10.1515/mim-2025-0031
Received November 1, 2025; accepted February 11, 2026;
published online April 29, 2026

Abstract: Oxygen (O_2) availability critically governs cellular physiology, however, standard cell culture systems often fail to recapitulate physiological oxygenation due to limited O_2 diffusion across the culture medium. Poorly defined O_2 equilibration dynamics *in vitro* can compromise reproducibility and contribute to experimental variability. Here, we employ live-cell fluorescence lifetime imaging microscopy (FLIM) using the genetically encoded O_2 reporter CMV-dUnOFLS – a PEST-destabilized UnaG-mOrange2 fusion protein – to monitor O_2 equilibration in real time. Frequency-domain FLIM (FD-FLIM) revealed rapid and reversible changes in UnaG fluorescence lifetime in Gli36 and CHO cells during cyclic variations of ambient O_2, reflecting culture medium oxygenation dynamics. Unexpectedly, in three different types of cell culture vessel, we noted a critical surface-area-to-volume (SA/V) ratio threshold of approximately 0.3 mm^{-1}, below which O_2 equilibration appeared to be delayed. Consequently, in 96-well plates, media volumes ≥100 µl significantly decelerated O_2 equilibration, while it occurred faster in 8-well imaging slides and 3.5 cm glass bottom dishes. Our findings demonstrate multiple factors critically influencing pericellular oxygenation and emphasize the necessity of real-time O_2 monitoring *in vitro*. The CMV-dUnOFLS reporter combined with FD-FLIM provides a powerful tool for assessing and optimizing O_2 dynamics in live-cell culture systems.

Keywords: *in vitro* oxygen equilibration; cellular oxygen sensor; FLIM reporter; FD-FLIM; TCSPC-FLIM

1 Introduction

Molecular oxygen (O_2) is a critical determinant of cellular function and strongly impacts processes such as cell survival, proliferation, metabolism and gene expression [1], [2]. *In vitro* cell culture models inevitably fail to replicate the complex oxygenation patterns of cells and tissues *in vivo*, leading to discrepancies between experimental outcomes [3]. In standard cell culture systems, O_2 from the gas phase diffuses through the medium to the cells. Although only scarcely studied and rarely documented, medium composition, height of the fluid column and a high oxygen consumption rate (OCR) may contribute to steep O_2 gradients, resulting in a hypoxic pericellular microenvironment even under ambient O_2 concentrations [4]. Variations in O_2 availability contribute to inconsistent cell behavior and signaling as well as poor reproducibility, limiting the physiological relevance of conventional culture models [3], [5].

Consequently, cells in culture have been claimed to be exposed to hyperoxia as well as hypoxia [3], [6], [7]. While both statements are encountered in the literature, they are rarely experimentally validated. Indeed, culturing cells in normobaric atmospheric versus normobaric reduced O_2 gas concentrations of 1 %–5 %, which are then referred to as normoxia and hypoxia respectively, is common practice. A recent landmark study focused on adipocytes provided experimental evidence for a critical medium height, which when exceeded, limits diffusive O_2 availability resulting in

***Corresponding author: Friedemann Kiefer**, European Institute for Molecular Imaging, University of Münster, Multiscale Imaging Center, Röntgenstraße 16, 48149 Münster, Germany,
E-mail: fkiefer@uni-muenster.de. https://orcid.org/0000-0002-3002-8237
Nadine Bauer, European Institute for Molecular Imaging, University of Münster, Röntgenstraße 16, 48149 Münster, Germany,
E-mail: nadine.bauer@uni-muenster.de.
https://orcid.org/0000-0002-4483-4205
Frank van den Boom, Nikon Europe B.V., Stroombaan 14, 1181 VX Amstelveen, The Netherlands, E-mail: frank.van.den.boom@nikon.com
Nico Marx and Karin B. Busch, Department of Biology, Institute of Integrative Cell Biology and Physiology, University of Münster, Schlossplatz 5, 48149 Münster, Germany,
E-mail: n_marx04@uni-muenster.de (N. Marx),
buschkar@uni-muenster.de (K. B. Busch).
https://orcid.org/0000-0003-3745-261X (N. Marx).
https://orcid.org/0000-0003-0525-0191 (K. B. Busch)
Gerhard Holst, Excelitas PCO GmbH, Donaupark 11, 93309 Kelheim, Germany, E-mail: gerhard.holst@excelitas.com

metabolic adaptation. Changes included a shift from oxidative to glycolytic metabolism, resulting in massive transcriptional changes and a reduction in TCA cycle metabolites [3].

A major obstacle for the derivation of quantitative data on cell oxygenation in culture are the complex instrumentation and costs associated with dynamic and reliable O_2 sensing at the cellular level. Planar sensor foils, dye-impregnated scaffolds and microsensor beads quantify cell culture oxygenation non-invasively and spatially resolved in real-time [8]–[11]. However, they frequently rely on specialized and costly measurement devices, while revealing only pericellular or intramatrix O_2 gradients, and in general do not reach cellular resolution. Quenched-phosphorescence O_2-sensing techniques, including nano sensors, quantum dots and metal complexes, have been constantly developed over the last two decades and enable the near real-time evaluation of intracellular oxygenation states [12]–[19]. This technique also allows the study of cell aggregates, as recently elegantly demonstrated in live tumor spheroids, where cell staining using advanced O_2-sensitive red/near-infrared (NIR) emitting nanoparticles revealed inverse O_2 gradient formation due to a glycolytic core in the presence of OxPhos-active cells at the periphery [20]. Limitations of intracellular quenched-phosphorescence O_2 sensing are posed by heterogenous membrane permeability, opposing robust cellular internalization, and in some cases the need for continuous probe administration – parameters that can vary substantially across replicates and experimental conditions. We refer to excellent reviews on the available O_2 sensing technologies [21]–[24].

Genetically encoded hypoxia or O_2 reporters based on luciferases or fluorescent proteins [25]–[29] overcome some of these constraints by allowing endogenous O_2 sensing with single-cell resolution. Although the temporal responsiveness of these reporters is inherently limited by the turnover of their functional protein domains, they provide a stable and continuous readout once integrated into the genome. More recently, a family of such genetically encoded O_2 sensors enables the direct monitoring of cellular oxygenation with both spatial and temporal resolution [30]–[35], offering a promising avenue toward dynamic and physiologically relevant O_2 measurements *in vitro*.

A novel addition to this sensor family is CMV-dUnOFLS, a dual-fluorescent reporter comprising a PEST-destabilized UnaG-mOrange2 fusion protein [33]. In well oxygenated cells, Förster resonance energy transfer (FRET) between UnaG and mOrange2 results in reduced UnaG fluorescence lifetime, while under hypoxic conditions mOrange2 fluorescence maturation is inhibited, resulting in decreasing FRET efficiency and increasing UnaG fluorescence lifetimes. Consequently, measurement of FRET efficiency, most efficiently performed using fluorescence lifetime imaging microscopy (FLIM), enables a graded assessment of the oxygenation status of living cells. CMV-dUnOFLS was initially calibrated in formaldehyde (FA)-fixed and live CHO and Gli63 cells across various O_2 concentrations ranging from 1 to 18 % O_2, using time-correlated single photon counting (TCSPC)-FLIM endpoint measurements of UnaG fluorescence lifetimes after 24–30 h incubation [33]. This initial description confirmed the capacity of CMV-dUnOFLS to distinguish defined O_2 environments, however, the sensor's dynamic response to oxygenation changes was not investigated.

Herein we demonstrate frequency-domain (FD)-FLIM measurements that dynamically monitor O_2 equilibration in cultured CMV-dUnOFLS-expressing Gli36 cells. In response to cycling ambient O_2 concentrations, live-cell FD-FLIM of CMV-dUnOFLS showed rapid, near real-time changes in UnaG fluorescence lifetime that reflected the equilibration of culture media under new steady-state O_2 levels. The kinetics of these lifetime changes varied depending on the applied medium volume and culture vessel type. These findings underscore the utility of genetically encoded O_2 reporters, such as CMV-dUnOFLS, to address limited O_2 equilibration of cell culture systems that may lead to pericellular hypoxia, possibly confounding outcomes of *in vitro* experiments. Integration of real-time monitoring should therefore provide a powerful approach to control O_2 equilibration dynamics in culture systems and thereby increase the physiological relevance and reproducibility of *in vitro* studies.

2 Materials and methods

2.1 Cell culture

The stable transgenic adherent glioma cell lines Gli36 CMV-dUnOFLS and CMV-dUnOFLS (G220A) as well as CHO CMV-dUnOFLS [33] were maintained in high glucose Dulbecco's Modified Eagle Medium (DMEM; Gibco) supplemented with 10 % (v/v) fetal calf serum (FCS), penicillin (100 U/ml)/streptomycin (0.1 mg/ml), 2 mM L-glutamine, 1 % (v/v) MEM non-essential amino acids (MEM NEAA 100×, PAN-Biotech) and 1 mM sodium pyruvate. Cells were cultured in a humidified incubator (95–100 % humidity) at 37 °C under 10 % CO_2 and normobaric atmospheric O_2 concentrations. To seed the cells in preparation for the herein described experiments or for passaging, cells were washed with 1X phosphate-buffered saline (PBS) and treated

with 0.05 % (w/v) trypsin/0.02 % (w/v) ethylenediaminetetraacetic acid (EDTA) in 1X PBS. The enzymatic reaction was stopped by adding cell culture media after completed cell detachment. Depending on the experimental setup, cells were seeded at a density of 2.5×10^4 cells/cm^2 into either 96-well flat glass bottom plates (1.5H, Cellvis (P96-1.5H-N)), 8-well glass bottom imaging slides (1.5H, ibidi (80,827)) or 3.5 cm glass bottom dishes (1.5H, WillCo (GWST-3512)). For live-cell FLIM imaging, cultures were maintained in Fluorobrite™ DMEM imaging media (Thermo Fisher Scientific), supplemented with penicillin (100 U/ml)/streptomycin (0.1 mg/ml), 2 mM L-glutamine, 1 % (v/v) MEM NEAA (100X, PAN-Biotech) and 1 mM sodium pyruvate.

2.2 Time-correlated single photon counting-FLIM

For TCSPC-FLIM, Gli36 cells stably expressing CMV-dUnOFLS or CMV-dUnOFLS (G220A) were seeded onto polystyrene cell culture dishes or glass cover slips and grown to approx. 40 % confluency. CMV-dUnOFLS expressing cells were subsequently incubated for an additional 24 h under either normobaric atmospheric O_2 or normobaric hypoxic conditions (1 % O_2). Following incubation, cells were fixed in 4 % (w/v) FA/PBS for 15 min at room temperature and washed with 1X PBS. For TCSPC-FLIM, using a PicoQuant MultiHarp 150 TCSPC device and PicoQuant PMA Hybrid detectors coupled to a Nikon AX-R confocal microscope, either on an upright Nikon AX-FN stand or on an inverted Nikon Ti2-E microscope, cells were covered with 1X PBS or mounted in Mowiol onto microscopy slides. Cells were imaged using a 20X water-dipping lens (Nikon Apo LWD 20× C WI, NA 1.00) or 20X dry objective (CFI PlanApo Lambda 20× D, NA 0.8), exciting with a 485 nm laser pulsed at 32 MHz. The lifetime signal was detected using a 520/35 nm emission filter.

2.3 Live-cell frequency-domain-FLIM

FD-FLIM of live CMV-dUnOFLS expressing Gli36 or CHO cells was performed using a Nikon Ti2-E epifluorescence microscope equipped with a humidified incubation chamber and gas mixing unit (OkoLab) for dynamic regulation of O_2 concentrations under culture conditions (37 °C, 10 % CO_2). The Nikon NIS-Elements software controlled automated image acquisition and O_2 changes during time-lapse experiments by employing the O_2 control and multipoint functions. Multiple fields of view per condition were acquired every 10 min for 1 h under normobaric atmospheric (18 %) O_2 and for 2 h under normobaric hypoxia-inducing (1 %) O_2 followed by reoxygenation at normobaric atmospheric (18 %) O_2 for 2 h. Images were recorded at 40X magnification (CFI S P-Fluor ELWD ADM 40× C, NA 0.6) using a FD-FLIM camera pco.flim X (1,008 × 1,008 pixel, 5 µm × 5 µm pixel size, dynamic range of 1:1,024, modulation frequency range of 5 kHz–40 MHz) with a fast modulatable CMOS sensor [37]–[39]. Upon excitation at 488 nm using a pco.flim laser unit (200 mW CW power with 3 mm liquid light guide output), lifetimes were recorded at 525/50 nm.

2.4 Trypan blue dynamic mixing in liquid phase

2 µl of a 0.4 % (v/v) trypan blue solution (Sigma-Aldrich (T8154)) were automatically infused at a speed of 4 µl/min via a glass capillary into an 8-well glass bottom imaging slide (1.5H, ibidi (80,827)) holding 200 µl of dH_2O, using a stereotactic injector (Stoelting Quintessential Stereotaxic Injector (QSI™)). Trypan blue distribution in the aqueous phase was monitored by time-lapse imaging using a Nikon Ti2-E widefield microscope with a 4X objective (CFI Plan Fluor DL 4X F, NA 0.13). A single field of view was observed every 2 s under static conditions, starting before the trypan blue injection. The total observation time lasted at least 5 min. In order to quantify the observed dynamic equilibration of the solution, the dye gradient was analyzed using FIJI by ImageJ [39]. To determine whether the observed mixing kinetics are dominated by either convection or diffusion, the theoretical diffusion-driven movement of trypan blue within the herein described experimental setup was calculated according to Fick's first law [40]:

$$J = -D\left(\frac{\Delta c}{\Delta x}\right) \tag{1}$$

With J as the diffusion flux (mol/(m^{2}s)), D as the diffusion coefficient of trypan blue (2.21×10^{-6} m^2/s) as experimentally determined by Inglesby & Zeronian in D_2O at 30 °C [41], Δc as the difference in concentration at two different points in space (mol/m^3) and Δx as the total difference between those points (mm). While J and Δc were experimentally determined by our dataset using Lambert–Beer's law, we calculated Δx, the theoretical diffusion-driven movement of trypan blue, *via*

$$\Delta x = -\left(\frac{D \cdot \Delta c}{J}\right). \tag{2}$$

2.5 Image analysis

Fluorescence intensity, brightfield and FLIM imaging data were analyzed using FIJI by ImageJ [39] and the Nikon NIS-Elements imaging and analysis software. Quantification of UnaG lifetimes based on the TCSPC-FLIM measurements

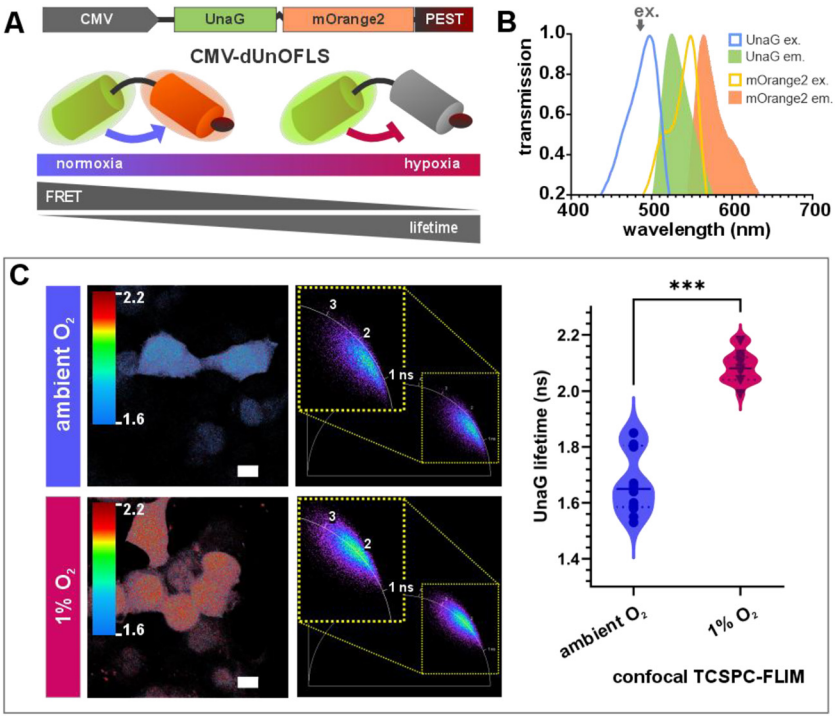

Figure 1: Principle of FLIM-based cellular O_2-sensing using the genetically encoded sensor CMV-dUnOFLS. (A) Schematic representation of the FLIM-sensor CMV-dUnOFLS. The UnaG-mOrange2 fusion protein is expressed under a constitutive cytomegalovirus (CMV) promoter and destabilized by a C-terminal PEST degradation motif. UnaG serves as the O_2-independent FRET donor, whereas mOrange2 functions as the O_2-sensitive acceptor. Under normobaric atmospheric O_2 concentrations mOrange2 efficiently matures to the fluorescent form and FRET leads to a reduced UnaG lifetime. Under hypoxia, impaired mOrange2 fluorophore maturation inhibits FRET, stabilizing increased UnaG lifetime [33]. (B) Excitation (ex., open curves) and emission (em., filled curves) spectra of UnaG and mOrange2. The spectral overlap between UnaG emission and mOrange2 excitation confirms their suitability as a FRET-pair. (C) Confocal TCSPC-FLIM of FA-fixed CMV-dUnOFLS-expressing Gli36 cells after 24 h of ambient (normobaric atmospheric, 18 %) versus normobaric hypoxic (1 %) O_2 incubation. Depicted are the UnaG lifetimes (mean first arrival times in ns) and representative phasor plots (scale bars: 20 µm). ROI analysis (normoxia: $n = 13$, hypoxia: $n = 19$) revealed a significant increase of UnaG lifetimes under O_2 deprivation (*** indicates significance $p < 0.001$).

were defined as mean first arrival times of photons per ROI (region of interest) using NIS-Elements. To extract phase lifetimes from live-cell FD-FLIM time-lapse datasets, ROIs corresponding to CMV-dUnOFLS-positive cells were defined by generating binary images of the fluorescence intensity stacks using FIJI. Binary stacks were processed by particle analysis (size: 100 − ∞, circularity: 0–1) to generate ROI masks, which were subsequently applied to the corresponding phase lifetime image stacks of the same field of view. Background subtracted lifetimes were obtained using the ROI Manager "Measure" function in FIJI. Fluorescence intensity images, FLIM images and phasor plots were extracted from time-lapse image stacks using NIS-Elements and FIJI. Mean phase lifetimes were calculated and visualized using Excel and GraphPad Prism Software. For the statistical analysis of the TCSPC-FLIM datasets, Welch's *t*-test was applied, with the significances represented by the p value (NJEM formatting; $^{***}p < 0.001$, $^{**}p = 0.001$–0.01, $^{*}p = 0.01$–0.05 and ns (not significant) $p \geq 0.05$). Second order polynomial smoothing of the UnaG lifetimes extracted from FD-FLIM time-lapse experiments was performed by averaging in consideration of 10 neighboring values without differentiating or integrating the raw data points. Statistical analysis of the FD-FLIM time-lapse experiments was conducted using a two-way ANOVA with a mixed-effects model. The interaction term (time × condition (media volume)) was evaluated to quantify the influence of media volume on lifetime dynamics over time and to determine whether O_2 equilibration kinetics differed significantly between conditions.

2.6 Oxygen consumption measurements

U87 ΔEGFR wildtype, Gli36 wildtype, Gli36 CMV-dUnOFLS and CMV-dUnOFLS (G220A) as well as CHO wildtype, CHO CMV-dUnOFLS and CMV-dUnOFLS (G220A) cell lines were seeded into XFe96/XF Pro Cell Culture 96-well microplates (Agilent) at a density of 2.5×10^4 and 5×10^4 cells/cm^2. Quantifications of OCRs were performed at 37 °C *via* an

extracellular flux analyzer (Seahorse XFe96, Agilent) using the Seahorse XF Cell Mito Stress Test Kit (Agilent) according to the manufacturer's protocol. Basal, ATP-synthase dependent and maximal respiration were determined by sequential addition of oligomycin (1.5 µM), carbonyl cyanide-*p*-trifluoromethoxyphenylhydrazone (FCCP; 2 µM) and rotenone (0.5 µM)/antimycin A (0.5 µM). Analysis and OCR calculation was conducted using the seahorse software Wave (Agilent).

3 Results

3.1 The sensor protein dUnOFLS allows monitoring of oxygen equilibration in cultured cells by live-cell FD-FLIM

The FLIM-based genetically encoded cellular O_2 sensor CMV-dUnOFLS was previously shown to reliably react to normobaric O_2 concentrations between 1 and 18 % O_2 (Figure 1A and B) [33]. However, its characterization was limited to endpoint measurements of live and FA-fixed cells following 24 h of incubation at defined O_2 tensions using confocal TCSPC-FLIM. Here, we were able to confirm the previously reported increase in UnaG lifetime in dUnOFLS under hypoxic conditions, from 1.675 ns in normobaric atmospheric O_2 to 2.087 ns in 1 % O_2 (Figure 1C), demonstrating suitability as a cellular oxygenation sensor. To confirm that the observed changes in UnaG lifetime were due to directly altered O_2 availability and not due to cellular metabolic adaptation to hypoxic or atmospheric conditions in the presence of high glucose medium and pyruvate, we also again validated the mOrange2 maturation-deficient donor-only control construct CMV-dUnOFLS (G220A), which displayed no significant difference in UnaG lifetimes between normobaric hypoxic and normoxic oxygenation states (Figure S1) [33].

Given the enhanced turn-over to be expected for the PEST-sequence containing sensor fusion protein, we wondered if response times of the sensor CMV-dUnOFLS were sufficiently short to follow O_2 equilibration kinetics by live-cell microscopy during O_2-switching experiments. Attracted by the ease and speed of measurement and the increased capacity for multiplexed image acquisition, we switched to lifetime determination in the FD. Therefore, we employed a FD-FLIM camera coupled to an epifluorescence microscope equipped with an incubation chamber (Figure 2), which allowed us to dynamically monitor the signal kinetics of

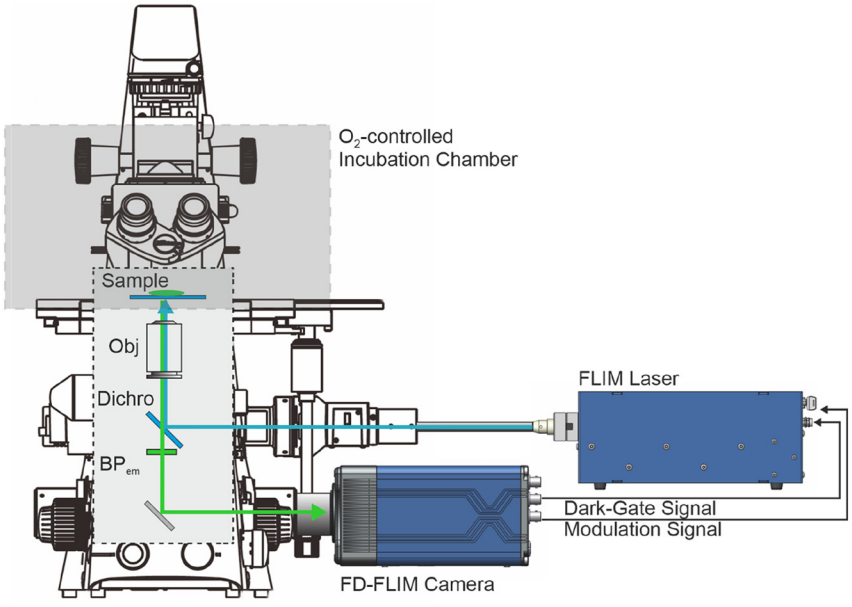

Figure 2: Scheme of the widefield FD-FLIM setup used in this study. The pco.flim laser depicted on the right receives its steering modulation and dark-gate signals (laser enable) from the pco.flim X camera system. Excitation laser light (488 nm) passes a mild diffusor (not drawn) and is coupled into a 3 mm liquid light guide, which annihilates coherence and guides the excitatory light into the epifluorescence input of an inverted Nikon Ti2-E fluorescence microscope, equipped with an O_2-controlled incubation chamber. Excitation light is reflected by a dichroic mirror (Dichro) (495 nm longpass filter) into the objective (Obj) to illuminate the sample, which is also blocking light $\leq$ 495 nm for exclusive detection of the emitted photons. Fluorescence emission collected by the objective is projected through the dichroic mirror and an emission bandpass filter (BP_{em}: 525/50 nm) and finally reflected by a silver mirror towards the camera port of the pco.flim X camera. The entire setup is controlled by the Nikon NIS elements software, which was also employed for lifetime determination.

CMV-dUnOFLS-expressing Gli36 cells grown in glass bottom 96-well plates during transitions between oscillating O_2 concentrations. Here we applied sequential transitions between normobaric ambient (1 h), normobaric hypoxic (2 h) and normobaric ambient (2 h) O_2 concentrations (18 % O_2 ⇨ 1 % O_2 ⇨ 18 % O_2). To probe the impact of the media column height atop the cells, we added media volumes between 30 µl and 350 µl corresponding to liquid column heights between 0.98 mm and 10.63 mm and determined UnaG lifetimes during the O_2 transitions every 10 min (Figure 3A). Notably, independent of the media volume UnaG lifetime started to adapt within 20 min after transitioning to the new O_2 concentration, with a tendency to stabilize during the following 3 h (Figure 3B). In agreement with the liquid column forming a diffusion barrier for O_2, UnaG lifetime changes were increasingly delayed with increasing media volume. This was particularly notable for culture volumes ≥100 µl, suggesting that while O_2 dissolved in the higher media columns still reached the cells alleviating the hypoxic state, the reduced gradient steepness resulted in a diminished flux. To highlight these differences, we generated denoised mean phase lifetime plots of the time-series data that preserved the overall signal kinetics by applying second order polynomial smoothing (Figure 3C). Compared

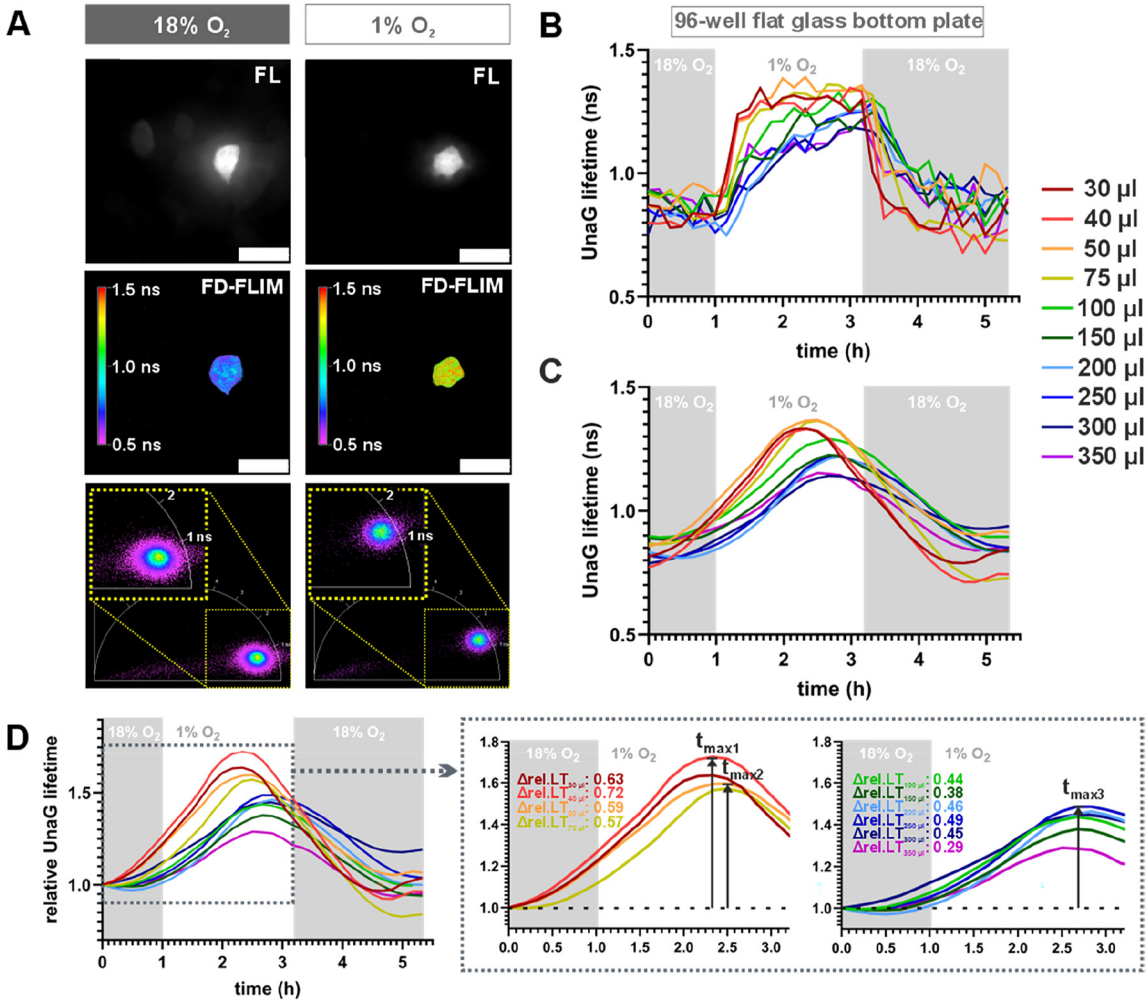

Figure 3: The genetically encoded O_2 sensor CMV-dUnOFLS revealed a pronounced impact of media column height on O_2 equilibration dynamics in 96-well plates. Gli36 cells stably expressing CMV-dUnOFLS were cultured in 96-well flat glass bottom plates and maintained in various media volumes ranging from 30 to 350 µl. UnaG fluorescence lifetimes were monitored by live epifluorescence FLIM in the frequency domain (FD) during sequential shifts between normobaric atmospheric and hypoxic conditions (18 % O_2 ⇨ 1 % O_2 ⇨ 18 % O_2). (A) Representative fluorescence intensity (FL) images, FD-FLIM images and corresponding phasor plots are shown (scale bars: 100 µm). (B) Mean UnaG lifetimes and (C) corresponding smoothed average traces demonstrate a marked influence of media height on O_2 equilibration dynamics within 96-well plates (fields of view, $n = 4$). (D) The normalized smoothed trajectories highlight the timepoints of maximal changes (t_{max}) of the relative UnaG lifetimes (Δrel.LT) within the various culture volumes, allowing to summarize three major dynamics at t_{max1} (2.3 h, 30 and 40 µl), t_{max2} (2.5 h, 50 and 75 µl) and t_{max3} (2.7 h, ≥ 100 µl) respectively.

to the smallest volumes (30 and 40 µl, $t_{max1} = 2.3$ h), the maximum of the resulting curve was delayed for larger volumes by approx. 12 min (50 and 75 µl, $t_{max2} = 2.5$ h) and 24 min (≥100 µl, $t_{max3} = 2.7$ h) respectively, highlighting the major variation in the dynamic changes of UnaG lifetime based on the applied culture media volume within 96-well plates (Figure 3D). The largest volumes (≥300 µl) showed no further increase when compared to smaller media heights, however, the relative change in UnaG lifetime (Δrel.LT = rel.LT$_{max}$ − rel.LT$_{t0}$) was minimal for 350 µl. In line with this, statistical analysis demonstrated that the time-course profiles obtained for the smallest media volumes (30 and 40 µl) differed significantly from those measured at volumes ≥100 µl. For intermediate volumes (50 and 75 µl), significant differences were detected only in comparison to the 300 µl-condition, while no significant differences were observed among media volumes ≥100 µl when compared with any larger column heights (Table S1).

Upon incubation under comparable conditions, Gli36 cells expressing the control construct CMV-dUnOFLS (G220A) also showed a measurable lifetime response to O_2 switching (Figure S2). However, the signal barely exceeded the background fluctuation and showed no volume dependent delay. It potentially reflected adaptive and metabolic cellular responses to altered oxygenation rather than direct sensor effects. Finally, to demonstrate a more general applicability of our sensor, we repeated the live-cell FD-FLIM measurements with CMV-dUnOFLS-expressing CHO cells, which showed similarly rapid and pronounced lifetime shifts during O_2 cycling (Figure S3). Also in this cell line, the maxima of the mean phase lifetime plots showed the above described temporal delay between minimal (30 and 40 µl), intermediate (50 and 75 µl) and larger media volumes (≥100 µl).

3.2 Parameters affecting oxygen equilibration in cell culture systems

Equilibration of ambient O_2 in the gas phase by passive diffusion is driven by the concentration gradient between the O_2 dissolved at the surface and the concentration at the bottom of the media column, where O_2 is consumed. Consequently, equilibration is inversely proportional to the diffusion distance, i.e. the height of the media column. Knowledge of the cellular OCR allows the calculation of the maximal diffusion distance that would replenish cellular O_2 consumption, based on Fick's law. Accordingly, we determined the cellular OCR at basal respiration of the cells used in this study as 59 amol/s/cell (29.5 fmol/s/mm^2) for Gli36 wildtype cells and 68.17 amol/s/cell (34 fmol/s/mm^2) for CHO wildtype cells (Figure S4) and calculated the corresponding cell type-specific maximal diffusion distances of 16.5 and 14.3 mm, based on the experimentally determined O_2 diffusion coefficient of Inglesby & Zeronian [41]. This suggests that these cell lines, when grown in 96-well plates with the maximal medium volume (350 µl, media column height of 10.6 mm), should not encounter persistent hypoxia. However, as our results show that varying column heights indeed seemed to influence oxygenation dynamics, we aimed to consider further parameters that may impact the involved equilibration kinetics.

Tissue culture vessels possess a wide variety of geometries, which, depending on the culture volume, result in largely varying ratios of media column height to culture surface area. We were wondering if culture vessel geometry impacted on O_2 equilibration, e.g. by an increased occurrence of convective or mixing fluid motion in vessels with a high surface area to volume ratio at common culture volumes. To exemplify these differences, we outlined the dimensions of three selected, commonly used cell culture vessels, 96-well plates, 8-well imaging slides and 3.5 cm petri dishes (Figure 4A) and annotated the resulting averaged surface area to volume (SA/V) ratios in Figure 4B. In 96-well plates a culture volume of 30 µl results in a media column height of 980 µm, i.e. a SA/V ratio of approx. 1 mm^{-1}. This arithmetic average ignores the inevitable fluid meniscus formation, therefore real media column height in the center of the well is likely significantly lower. Every addition of 30 µl medium add approx. another 1 mm of fluid column height, with decreasing impact of meniscus formation. At the maximal culture volume of 350 µl the fluid column approaches 10.63 mm height, i.e. a SA/V ratio of 0.10 mm^{-1}. In a 3.5 cm dish, with a range of culture volumes between 1.5 ml and 4 ml the SA/V ratio varies between 0.64 and 0.24 mm^{-1}.

Diffusive O_2 transport through the aqueous phase in cell culture systems strictly only applies under static conditions. In real life scenarios various environmental factors, like vibration and thermal inhomogeneities of the incubated volume may cause fluid motion ultimately resulting in convective mixing. Using time-lapse widefield microscopy and trypan blue as a proxy, we aimed to visualize kinetic mixing, which could contribute to equilibration within the aqueous phase in a chamber of an 8-well imaging slide. We detected a spread of the forming dye front over a distance of approx. 2.61 mm during the observed timeframe (Figure 4C). Application of Fick's first law yielded a theoretical diffusion distance of 2.85 mm for trypan blue molecules, under the assumption that the observed equilibration of the solution was governed solely by passive diffusion kinetics (Figure 4C). These data therefore suggest that solution equilibration within cell culture vessels under static conditions

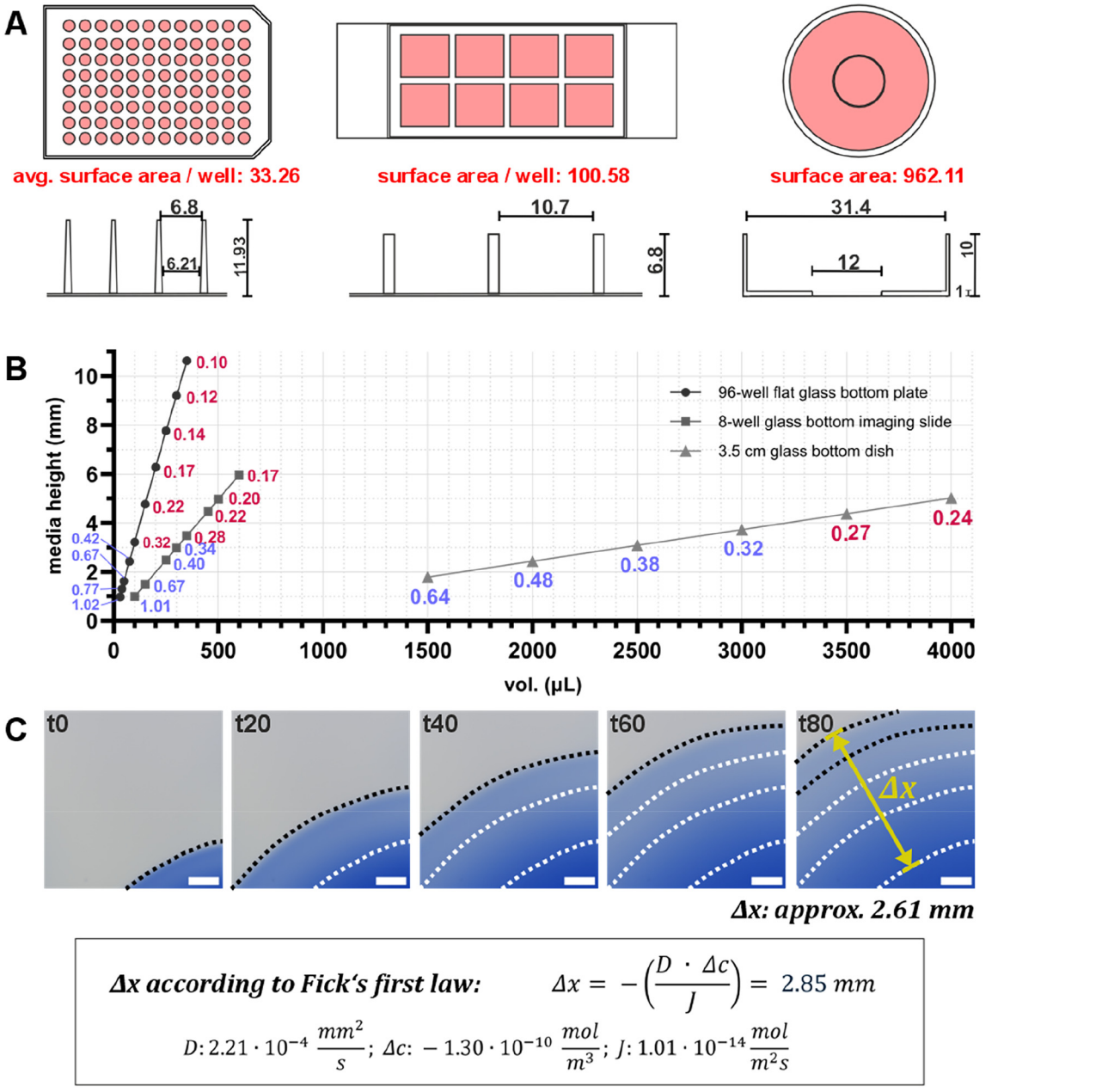

Figure 4: Geometric parameters of three common cell culture vessel types. (A) Dimensions (in mm) and respective surface areas (in mm^2) of 96-well flat glass bottom plates (1.5H, Cellvis (P96-1.5H-N)), 8-well glass bottom imaging slides (1.5H, ibidi (80,827)) and 3.5 cm glass bottom dishes (1.5H, WillCo (GWST-3512)). (B) Relationship of media volume and height of the resulting fluid column in different cell culture vessels. Annotations indicate the calculated surface-area-to-volume ratios ($SA/V = mm^2/mm^3$) in mm^{-1}. Color-coding of ratios indicates fast (blue) or slow (red) media O_2 equilibration, which was reflected by the experimentally determined, delayed arrival at the new steady-state after a normobaric switch in O_2 concentration. Media heights and surface areas were approximated without consideration of the cohesive forces, which result in concave meniscus formation at aqueous surfaces. (C) Kinetic distribution of trypan blue within an aqueous phase. The expanding, nascent dye front generated by gentle infusion of a concentrated trypan blue volume into 200 µl dH_2O within an 8-well glass bottom imaging slide was visualized using widefield microscopy. Images were recorded every 2 s. According to Fick's first law, the theoretical diffusion-driven distance (Δx) of trypan blue within the herein observed conditions and timeframe results in a distance of 2.85 mm (D, diffusion coefficient [41]; Δc, difference in concentration at two different points in space; J, diffusion flux). The experimentally determined distance closely approximated this value with 2.61 mm, scale bar: 500 µm.

is predominantly governed by diffusion, whereas convective and kinetic effects have only a minor impact on the observed fluid equilibration.

We still wondered to what extent varying SA/V ratios contributed differentially to O_2 equilibration of cell cultures within the different culture vessel geometries. Having

demonstrated the potential of dUnOFLS to monitor cellular oxygenation dynamically with cellular resolution, we employed it to also record O_2 equilibration in ibidi 8-well imaging slides and 3.5 cm glass bottom dishes.

3.3 Changes in media height caused less pronounced effects on oxygenation when cultures were kept in larger diameter culture vessels

In 8-well imaging slides variation of the media volume (100–600 µl) had a less pronounced impact on the kinetic of UnaG lifetime changes in dUnOFLS-expressing Gli36 cells after O_2 switching when compared to 96-well plates. While media volumes ≤300 µl displayed fast switching kinetics ($t_{max} = 2.4$ h) in response to new steady-state O_2 concentrations, higher media volumes (≥350 µl) resulted in a slightly delayed equilibration of UnaG lifetimes upon de- and reoxygenation ($t_{max} = 2.7$ h; Figure 5A and B). However, statistical analysis indicated that the differences between the time-course datasets did not reach an appreciable level of significance (Table S2). Nevertheless, our sensor system detected a threshold for fast O_2 equilibration at media column heights $\lessapprox$3 mm, or a SA/V ratio $\gtrapprox$0.34 mm^{-1}, in 8-well imaging slides with a surface area of 100.58 mm^2 per well. This ratio compares well with the threshold identified for 96-well plates (Figure 4B).

In 3.5 cm glass bottom dishes, increasing the media volume from 1,500 to 4,000 µl did have mild, but significant effects on the culture media oxygenation kinetics (Figure 5C and D; Table S3). UnaG lifetimes adapted within 1 h when transitioning from atmospheric to hypoxic O_2 concentrations, with a t_{max} at approx. 2.5 h for volumes ≤3 ml and 2.7 h for volumes ≥3,500 µl, while reoxygenation was meaningfully delayed at higher media volumes ≥3,500 µl. For 3.5 cm glass bottom dishes, media volumes of 3,500 µl correspond to a column height of approx. 4.4 mm and, given a surface area of 960 mm^2, a SA/V ratio of approx. 0.27 mm^{-1} (Figure 4B). Thus, SA/V ratios $\lessapprox$0.27 mm^{-1} indicate a threshold for potentially delayed equilibration of culture media during O_2 transitions within 3.5 cm glass bottom dishes (Figure 4B). FLIM images and phasor plots of CMV-dUnOFLS-expressing Gli36 cells cultured in 8-well imaging slides (Figure S5A) and 3.5 cm glass bottom dishes (Figure S5B) represent the observed UnaG lifetime shifts in response to ambient O_2 changes.

Collectively, these findings demonstrate that FD-FLIM of CMV-dUnOFLS-expressing cells provides reliable detection of O_2 equilibration dynamics in *in vitro* systems – including consistent performance across all cells in independent fields of view (Figure S6) – and further revealed that the influence of media heights on O_2 diffusion progressively diminishes with increasing SA/V ratios.

4 Discussion

Here we have exploited the recently described, genetically encoded O_2 sensor CMV-dUnOFLS to monitor O_2 equilibration in cultured cells after normobaric switching of the O_2 concentration in the incubator gas phase from atmospheric concentration to 1 % and back. The sensor protein dUnOFLS is comprised of a PEST-sequence-destabilized fusion of the green fluorescent protein UnaG, which acquires its fluorescent state independent of the presence of molecular O_2 in a complex with bilirubin, and mOrange2, which matures in an O_2-dependent fashion [33], [43]–[45]. UnaG and mOrange2 form an efficient FRET pair upon expression from a ubiquitously active cytomegalovirus (CMV) promoter element, allowing a graded readout of cell oxygenation. The sensor protein therefore avoids the potentially unrecognized sensor failure inherent to sensor systems that express a fluorescent marker, selectively in either oxygenated or hypoxic cells. Taking advantage of its inherent insensitivity to concentration changes and background fluorescence, we employed live-cell FLIM imaging to determine UnaG lifetimes of cell lines stably expressing dUnOFLS.

In a first step, we determined the lifetime of UnaG in the context of the sensor under normobaric atmospheric and 1 % O_2 confocally by TCSPC-FLIM. The measured values of dUnOFLS of approx. 1.7 ns (ambient) and 2.1 ns (at 1 % O_2 and measured for the acceptor-deficient control dUnOFLS (G220A)) were in excellent agreement with our own previous measurements and published data [33], [45], [46]. Unexpectedly, our measurement revealed a previously unnoted biphasic lifetime distribution, which may reflect the two described reversibly interconvertible UnaG fluorescent states [47]. In our previous study, we directly fitted the TCSPC data by applying a biexponential fitting model and regarding the acceptor-deficient control lifetimes of dUnOFLS (G220A) as a fixed monoexponential variable. This provided a single time constant of 2.2 ns, which however missed the biphasic distribution revealed by direct plotting of the mean first photon arrival times.

The capacity of dUnOFLS to report oxygenation in cultures with cellular resolution, potentially opens the possibility to dynamically assess O_2 equilibration by live-cell microscopy, depending on the cellular turnover of the sensor.

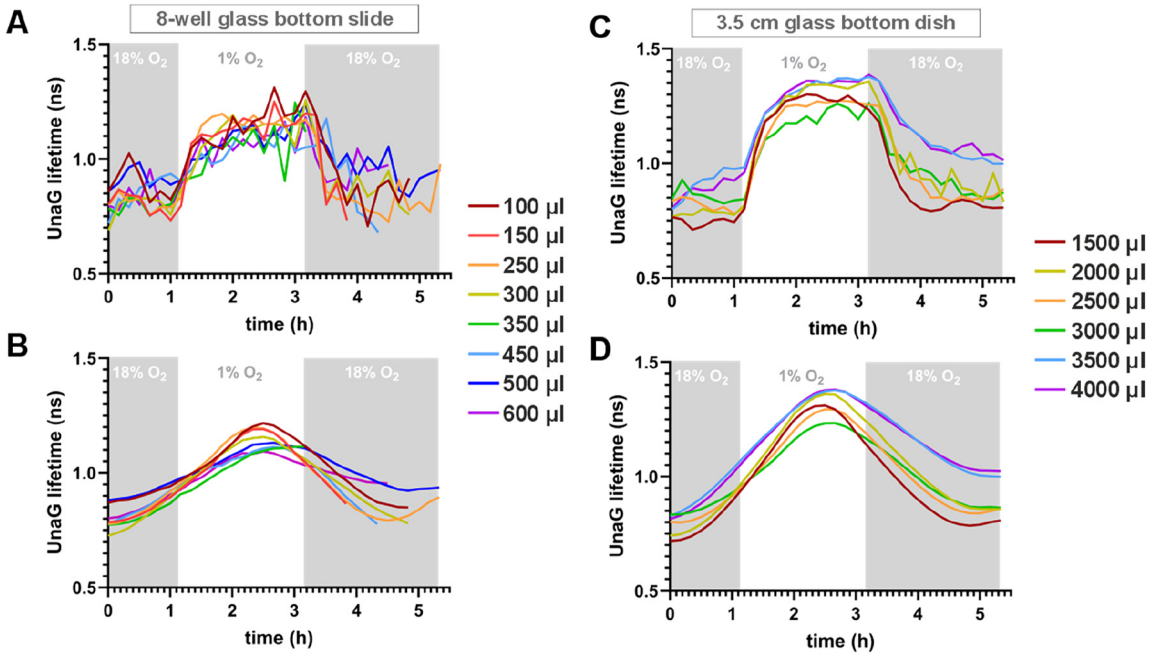

Figure 5: Changes in media volume resulted only in minor variations of O_2 equilibration dynamics in 8-well imaging slides and 3.5 cm glass bottom dishes. Gli36 cells stably expressing CMV-dUnOFLS were cultured in (A, B) varying media volumes ranging from 100 to 600 µl in 8-well glass bottom imaging slides or (C, D) various media volumes ranging from 1.500 to 4.000 µl in 3.5 cm glass bottom dishes. UnaG lifetimes during sequential normobaric changes of the O_2 concentration from 18 % O_2 to 1 % O_2 and back to 18 % O_2 were determined by FD-FLIM. (A, C) Mean UnaG lifetimes and (B, D) corresponding averaged lifetime changes (smoothed average traces) indicated only a minimal dependence of cellular oxygenation on media volumes within the 8-well imaging slides (fields of view, $n = 3$) and in 3.5 cm glass bottom dishes (fields of view, $n = 10$).

To assess the dUnOFLS sensor response after normobaric changes in ambient O_2 concentration and probe the influence of media volume and hence culture vessel geometry, we switched from TCSPC measurements to FD lifetime determination using a dedicated FLIM camera system, which offers increased measurement speed and improved capacity for multiplexed image acquisition. Satisfactorily, after O_2 concentration switching, dUnOFLS displayed a sufficiently short reaction time of approx. 20 min and a clear lifetime change response of about 0.5 ns. Taken together, these parameters allowed meaningful dynamic measurements. However, the UnaG lifetime determined for dUnOFLS in the FD at normobaric atmospheric conditions of approx. 0.85 ns differed significantly from the approx. 1.7 ns lifetime determined by TCSPC. Possible reasons could be of technical nature, like differences in the principle and precision of the instrument calibration method or consequences of the inherent differences between confocal and epifluorescence-based acquisition used for the here presented TCSPC and FD measurements respectively. Also, epifluorescence acquisition in the FD records a vastly larger excitation volume compared to confocal TCSPC. Recently, Mukherjee et al. [48] reported subtle phototoxic effects of widefield FD-FLIM in HeLa and Cos7 cells when directly comparing FD- and TCSPC-FLIM measurements. In their study, light activation of an imaging medium component resulted in the degradation of a signaling agonist, identifying the molecular composition of imaging media as a potential source of variability in lifetime measurements [48]. In contrast, CMV-dUnOFLS-expressing cells exhibited consistent results across TCSPC-FLIM measurements live in cell culture media and under FA-fixed conditions in PBS or Mowiol. Our herein reported discrepancies between FD- and TCSPC-FLIM-derived UnaG lifetimes are therefore more likely attributable to differences in imaging modality. Furthermore, UnaG lifetime has been reported to vary depending on the cellular localization of the protein, which is likely even more pronounced in fusion proteins like dUnOFLS [46] and might contribute to the small, detectable change of approximately 0.15 ns in the lifetime of the dUnOFLS (G220A) control sensor. We had not detected a corresponding change in TCSPC endpoint measurements, suggesting that it likely reflects metabolic adaptations and possibly internal changes in protein localization and organelle distribution that are only revealed in real-time FD measurements and probably do not reflect real sensor responses.

O_2 transport in cell cultures is generally assumed to occur through diffusive flux, which, according to Fick's first

law, is directly proportional to the concentration gradient forming over the media fluid column. The media column height at which O_2 flux matches the cellular OCR is generally considered as the culture volume, above which cells grow under persistent hypoxia. Maximal diffusive flux is reached, at a media volume where the cellular OCR reduces peri-mitochondrially available O_2 to near zero. Under these conditions the concentration gradient equals the O_2 concentration at the gas interface, 0.181 mM [49]. Due to its exceptionally high affinity for O_2, cytochrome *c* oxidase is still capable of extracting O_2 and reaching half maximal activity at values lower than 0.01 mM O_2 [49]. However, due to the significantly lower affinity of other O_2 consuming enzymes, notably prolyl hydroxylases (approx. 0.25 mM), cells may already mount a response to consumptive O_2 depletion at distinctly higher O_2 concentrations [50].

Tan et al. calculated the critical media height based on an OCR of 200 fmol/mm^2/s for adipocytes as 2.43 mm [3]. Wagner et al. report OCRs spanning nearly three orders of magnitude, covering the range from single to three digit numbers in amol/cell/s [51]. We noted significant variation in the cellular OCRs reported for glioblastoma cell lines. Vlashi and coworkers reported the OCRs of U87 and GBM147 glioblastoma cell lines at ∼9,000 pmol/min/10^6 cells (∼150 amol/cell/s) [52], while Sharapova et al. reported 35 to 100 amol/s/cell [53]. These values as well as the values we determined for Gli36 (59 amol/s/cell) and CHO cells (68 amol/s/cell) lie well within the range described by Wagner et al. [51]. The higher OCR of CHO cells may be a consequence of Warburg effect active in the tumor cell line. In contrast, Arthurs et al. report OCRs for glioblastoma cell lines around 150–200 pmol/cell/s, which is approx. 10^4–10^5 higher compared to the otherwise reported literature value [54].

While our measurements indicate that under all conditions investigated in this study, diffusive O_2 flux would compensate the OCR, the discrepancy in reported OCRs impressively highlights the requirement for a reproducible experimental method to determine cellular oxygenation. Using stable expression of dUnOFLS, we here show a distinct delay of O_2 equilibration in 96-well plates dependent on the media volume. This effect was less pronounced in 8-well imaging slides and 3.5 cm dishes. The rapid kinetic, i.e. a detectable change in dUnOFLS lifetime after already 20 min, was surprising as it essentially relies on protein turnover. However, an equally swift response in CHO cells demonstrated that the effect was not specific to tumor cell lines.

Remarkably, independent of the vessel geometry, oxygenation trended to be delayed at SA/V ratios <0.3. Our trypan blue-based assays performed in 8-well imaging slides at SA/V ratios <0.3 under static conditions are in agreement with equilibration predominantly being driven by passive diffusion. In contrast, the presented live-cell FLIM experiments involved sequential acquisition of multiple fields of view, necessitating repeated automated mechanical movement of the culture vessels. Such perturbations are likely to induce kinetic mixing phenomena, including convective flow, thereby facilitating enhanced equilibration dynamics during multipoint time-lapse imaging. Furthermore, the SA/V value we have determined here may be specific for the live-cell incubation chamber at hand and might need to be independently determined for different incubators and experimental setups. Growing cells at low media volumes clearly reduces the risk of hypoxic episodes, however, at the risk of early nutrient depletion or even fluid evaporation. On the other hand, cells grown at the maximally recommended culture volumes showed clearly delayed O_2 equilibration.

5 Conclusions

Taken together, we show that cycling changes in the oxygenation state of tissue cultures can be monitored by lifetime measurements of sensor proteins like dUnOFLS with a cellular response time of approx. 20 min. Due to the fast evaluation process, the phasor approach and lifetime determination by FD-FLIM are particularly well suited for this task. We also provide evidence that fluid equilibration of static cell cultures is indeed predominantly governed by passive diffusion. However, our FD-FLIM measurements indicated that diffusive gas equilibration appeared to only insufficiently provide O_2 to cells that grow at culture conditions below a SA/V ratio of approx. < 0.3. Our results highlight the value of experimental approaches that monitor cellular states including oxygenation in tissue cultures. Moreover, the applicability of dUnOFLS has previously been demonstrated not only *in vitro* but also *ex vivo* in an intracranial glioma xenograft model [33]. In light of the rapid dynamic sensor responsiveness revealed in the herein presented study, we propose that in the future FD-FLIM could also be employed to intravitally monitor tissue oxygenation in preclinical disease models using dUnOFLS.

Acknowledgments: We gratefully acknowledge Femke Testroet and Dirk Reinhardt from the European Institute for Molecular Imaging for assisting with the technical procedure of the tryplan blue-based diffusion experiments. We thank Baris Tursun, Molecular Cell Biology of Animals, University of Hamburg, for granting access to the Nikon AX-R

FLIM and Ti2 microscope, used for additional TCSPC-FLIM measurements.

Research ethics: Not applicable.

Informed consent: Informed consent was obtained from all individuals included in this study.

Author contributions: F.K. and N.B. designed the experiments and wrote the manuscript. N.B. conducted the experiments and F.v.d.B. performed confocal TCSPC-FLIM measurements. N.M. supported with performing the oxygen consumption measurements. K.B.B. provided access to the seahorse analyzer. G.H. assisted with the technical set-up of the FD-FLIM live-cell experiments. G.H. and F.v.d.B. actively contributed to the writing process of the manuscript. All authors have accepted responsibility for the entire content of this manuscript and approved its submission.

Use of Large Language Models, AI and Machine Learning Tools: None declared.

Conflict of interest: G.H. is an employee of Excelitas PCO GmBH which manufactures the camera system applied for the measurements presented in this article.

Research funding: F.K. and N.B. gratefully acknowledge funding by the Deutsche Forschungsgemeinschaft (CRC 1450-431460824). F.K. gratefully acknowledges the CRC 1607-501530074 (DFG) and the HORIZON EUROPE Marie Sklodowska-Curie Actions 1,01119613.

Data availability: The data that support the findings of this study are available on request from the corresponding author, F.K.

References

[1] D. Samanta, N. R. Prabhakar, and G. L. Semenza, "Systems biology of oxygen homeostasis," *WIREs Syst. Biol. Med.*, vol. 9, no. 4, 2017, Art. no. e1382.

[2] G. L. Semenza, "Life with oxygen," *Science*, vol. 318, no. 5847, pp. 62—4, 2007.

[3] J. Tan *et al*., "Limited oxygen in standard cell culture alters metabolism and function of differentiated cells," *EMBO J.*, vol. 43, no. 11, pp. 2127—65, 2024.

[4] R. H. Wenger, V. Kurtcuoglu, C. C. Scholz, H. H. Marti, and D. Hoogewijs, "Frequently asked questions in hypoxia research," *HP*, vol. 3, pp. 35—43, 2015.

[5] N. M. Mazure, "Oxygen shortage: Himalayan adventures in an incubator," *EMBO J.*, vol. 43, no. 11, pp. 2087—90, 2024.

[6] Z. J. Rogers *et al*., "Controlling pericellular oxygen tension in cell culture reveals distinct breast cancer responses to low oxygen tensions," *Adv. Sci.*, vol. 11, no. 30, 2024, Art. no. 2402557.

[7] R. Alva, G. L. Gardner, P. Liang, and J. A. Stuart, "Supraphysiological oxygen levels in mammalian cell culture: Current state and future perspectives," *Cells*, vol. 11, no. 19, 2022, Art. no. 3123.

[8] H. Välimäki *et al*., "Covalent immobilization of luminescent oxygen indicators reduces cytotoxicity," *Biomed. Microdevices*, vol. 22, no. 2, 2020, Art. no. 41.

[9] L. Wang, M. A. Acosta, J. B. Leach, and R. L. Carrier, "Spatially monitoring oxygen level in 3D microfabricated cell culture systems using optical oxygen sensing beads," *Lab Chip*, vol. 13, no. 8, pp. 1586—92, 2013.

[10] J. Jenkins, R. I. Dmitriev, K. Morten, K. W. McDermott, and D. B. Papkovsky, "Oxygen-sensing scaffolds for 3-dimensional cell and tissue culture," *Acta Biomater.*, vol. 16, pp. 126—35, 2015.

[11] C. J. Peniche Silva, G. Liebsch, R. J. Meier, M. S. Gutbrod, E. R. Balmayor, and M. van Griensven, "A new non-invasive technique for measuring 3D-Oxygen gradients in Wells during mammalian cell culture," *Front. Bioeng. Biotechnol.*, vol. 8, 2020, https://doi.org/10.3389/fbioe.2020.00595.

[12] A. V. Zhdanov, V. I. Ogurtsov, C. T. Taylor, and D. B. Papkovsky, "Monitoring of cell oxygenation and responses to metabolic stimulation by intracellular oxygen sensing technique," *Integr. Biol.*, vol. 2, no. 9, pp. 443—51, 2010.

[13] D. N. S. dos Santos, N. Naskar, E. Delgado-Pinar, K. Reess, J. S. Seixas de Melo, and A. Rueck, "Bromine indirubin FLIM/PLIM sensors to measure oxygen in normoxic and hypoxic PDT conditions," *Photodiagnosis Photodyn. Ther.*, vol. 45, 2024, Art. no. 103964.

[14] A. Shamirian, H. S. Afsari, A. Hassan, L. W. Miller, and P. T. Snee, "In vitro detection of hypoxia using a ratiometric quantum dot-based oxygen sensor," *ACS Sens.*, vol. 1, no. 10, pp. 1244—50, 2016.

[15] J. Lecoq *et al*., "Simultaneous two-photon imaging of oxygen and blood flow in deep cerebral vessels," *Nat. Med.*, vol. 17, no. 7, pp. 893—8, 2011.

[16] T. Schäfer *et al*., "Covalently platinated DNA oligonucleotides as ratiometric dioxygen sensors," *Bioconjugate Chem.*, vol. 36, no. 11, pp. 2487—96, 2025.

[17] C. Wu, B. Bull, K. Christensen, and J. McNeill, "Ratiometric single-nanoparticle oxygen sensors for biological imaging," *Angew. Chem. Int. Ed.*, vol. 48, no. 15, pp. 2741—5, 2009.

[18] T. Yoshihara, Y. Yamaguchi, M. Hosaka, T. Takeuchi, and S. Tobita, "Ratiometric molecular sensor for monitoring oxygen levels in living cells," *Angew. Chem., Int. Ed.*, vol. 51, no. 17, pp. 4148—51, 2012.

[19] R. I. Dmitriev *et al*., "Versatile conjugated polymer nanoparticles for high-resolution O2 imaging in cells and 3D tissue models," *ACS Nano*, vol. 9, no. 5, pp. 5275—88, 2015.

[20] A. C. Debruyne *et al*., "Live microscopy of multicellular spheroids with the multimodal near-infrared nanoparticles reveals differences in oxygenation gradients," *ACS Nano*, vol. 18, no. 19, pp. 12168—86, 2024.

[21] R. I. Dmitriev and D. B. Papkovsky, "Optical probes and techniques for O2 measurement in live cells and tissue," *Cell. Mol. Life Sci.*, vol. 69, no. 12, pp. 2025—39, 2012.

[22] N. Bauer and F. Kiefer, "Genetically encoded reporters to monitor hypoxia," in *Hypoxia: Methods and Protocols*, *Methods in Molecular Biology*, D. M. Gilkes, Ed., New York, NY, US, Springer, 2024, pp. 3—29.

[23] E. Roussakis, Z. Li, A. J. Nichols, and C. L. Evans, "Oxygen-sensing methods in biomedicine from the macroscale to the microscale," *Angew Chem. Int. Ed. Engl.*, vol. 54, no. 29, pp. 8340—62, 2015.

[24] D. B. Papkovsky and R. I. Dmitriev, "Imaging of oxygen and hypoxia in cell and tissue samples," *Cell. Mol. Life Sci.*, vol. 75, no. 16, pp. 2963—80, 2018.

[25] S. Youssef, W. Ren, and H.-W. Ai, "A genetically encoded FRET sensor for hypoxia and prolyl hydroxylases," *ACS Chem. Biol.*, vol. 11, no. 9, pp. 2492—8, 2016.

[26] P. V. Lidsky, K. A. Lukyanov, T. Misra, B. Handke, A. S. Mishin, and C. F. Lehner, "A genetically encoded fluorescent probe for imaging of oxygenation gradients in living Drosophila," *Development*, vol. 145, no. 4, 2018, Art. no. dev156257.
[27] Q. Lin, Y. Huang, F. J. Giordano, and Z. Yun, "Generation of a hypoxia-sensing mouse model," *Genesis*, vol. 58, nos. 3—4, 2020, Art. no. e23352.
[28] T. Misra *et al*., "A genetically encoded biosensor for visualising hypoxia responses in vivo," *Biol. Open*, vol. 6, no. 2, 2017, Art. no. 296, https://doi.org/10.1242/BIO.018226.
[29] D. Vordermark, T. Shibata, and J. M. Brown, "Green fluorescent protein is a suitable reporter of tumor hypoxia despite an oxygen requirement for chromophore formation," *Neoplasia (New York, N.Y.)*, vol. 3, no. 6, pp. 527—34, 2001.
[30] C. Schmitz, E. Potekhina, V. V. Belousov, A. Lavrentieva, and A. Lavrentieva, "Hypoxia onset in mesenchymal stem cell spheroids: Monitoring with hypoxia reporter cells," *Front. Bioeng. Biotechnol.*, vol. 9, 2021, Art. no. 611837.
[31] C. Schmitz *et al*., "Live reporting for hypoxia: Hypoxia sensor-modified mesenchymal stem cells as in vitro reporters," *Biotechnol. Bioeng.*, vol. 117, no. 11, pp. 3265—76, 2020.
[32] R. Erapaneedi, V. V. Belousov, M. Schäfers, and F. Kiefer, "A novel family of fluorescent hypoxia sensors reveal strong heterogeneity in tumor hypoxia at the cellular level," *EMBO J.*, vol. 35, pp. 102—13, 2016.
[33] N. Bauer *et al*., "Genetically encoded dual fluorophore reporters for graded oxygen-sensing in light microscopy," *Biosens. Bioelectron.*, vol. 221, 2023, Art. no. 114917.
[34] N. Bauer *et al*., "Therapy-induced modulation of tumor vasculature and oxygenation in a murine glioblastoma model quantified by deep learning-based feature extraction," *Sci. Rep.*, vol. 14, no. 1, 2024, Art. no. 1.
[35] A. Sattiraju *et al*., "Hypoxic niches attract and sequester tumor-associated macrophages and cytotoxic T cells and reprogram them for immunosuppression," *Immunity*, vol. 56, no. 8, pp. 1825—43.e6, 2023.
[36] R. Franke and G. A. Holst, "Frequency-domain fluorescence lifetime imaging system (pco.flim) based on a in-pixel dual tap control CMOS image sensor," in *Imaging, Manipulation, and Analysis of Biomolecules, Cells, and Tissues XIII*, SPIE, 2015, pp. 241—59.
[37] H. Chen, G. Holst, and E. Gratton, "Modulated CMOS camera for fluorescence lifetime microscopy," *Microsc. Res. Tech.*, vol. 78, no. 12, pp. 1075—81, 2015.
[38] K. Koren, M. Moßhammer, V. V. Scholz, S. M. Borisov, G. Holst, and M. Kühl, "Luminescence lifetime imaging of chemical sensors — a comparison between time-domain and frequency-domain based camera systems," *Anal. Chem.*, vol. 91, no. 5, pp. 3233—8, 2019.
[39] J. Schindelin *et al*., "Fiji: An open-source platform for biological-image analysis," *Nat. Methods*, vol. 9, no. 7, pp. 676—82, 2012.
[40] A. Fick, "Ueber diffusion," *Ann. Phys.*, vol. 170, no. 1, pp. 59—86, 1855.
[41] M. K. Inglesby and S. H. Zeronian, "Diffusion coefficients for direct dyes in aqueous and polar aprotic solvents by the NMR pulsed-field gradient technique," *Dyes Pigm.*, vol. 50, no. 1, pp. 3—11, 2001.
[42] A. Kumagai *et al*., "A bilirubin-inducible fluorescent protein from eel muscle," *Cell*, vol. 153, no. 7, pp. 1602—11, 2013.
[43] N. C. Shaner *et al*., "Improving the photostability of bright monomeric orange and red fluorescent proteins," *Nat. Methods*, vol. 5, pp. 545—51, 2008.
[44] S. Rogers, R. Wells, and M. Rechsteiner, "Amino acid sequences common to rapidly degraded proteins: The PEST hypothesis," *Science*, vol. 224, no. 4655, pp. 1343—6, 1986.
[45] X. Cao, *et al*., "Ultrafast internal conversion dynamics of bilirubin bound to UnaG and its N57A mutant," *Phys. Chem. Chem. Phys.*, vol. 21, no. 5, pp. 2365—71, 2019.
[46] V. V. Terekhova *et al*., "Enabling fluorescence lifetime imaging multiplexing using UnaG through its modification with canonical and noncanonical amino acids," *ACS Sens.*, vol. 10, no. 9, pp. 6687—99, 2025.
[47] Y. Shitashima, T. Shimozawa, A. Kumagai, A. Miyawaki, and T. Asahi, "Two distinct fluorescence states of the ligand-induced green fluorescent protein UnaG," *Biophys. J.*, vol. 113, no. 7, pp. 2805—14, 2017.
[48] S. Mukherjee, J. Klarenbeek, F. El Oualid, B. van den Broek, and K. Jalink, ""Radical" differences between two FLIM microscopes affect interpretation of cell signaling dynamics," *iScience*, vol. 27, no. 7, 2024, Art. no. 110268.
[49] T. L. Place, F. E. Domann, and A. J. Case, "Limitations of oxygen delivery to cells in culture: An underappreciated problem in basic and translational research," *Free Radic. Biol. Med.*, vol. 113, pp. 311—22, 2017.
[50] G.-H. Fong and K. Takeda, "Role and regulation of prolyl hydroxylase domain proteins," *Cell Death Differ.*, vol. 15, no. 4, pp. 635—41, 2008.
[51] B. A. Wagner, S. Venkataraman, and G. R. Buettner, "The rate of oxygen utilization by cells," *Free Radic. Biol. Med.*, vol. 51, no. 3, pp. 700—12, 2011.
[52] E. Vlashi *et al*., "Metabolic state of glioma stem cells and nontumorigenic cells," *Proc. Natl. Acad. Sci. U. S. A.*, vol. 108, no. 38, pp. 16062—7, 2011.
[53] G. Sharapova *et al*., "Mitochondrial protein density, biomass, and bioenergetics as predictors for the efficacy of glioma treatments," *Int. J. Mol. Sci.*, vol. 25, no. 13, 2024, Art. no. 7038.
[54] A. L. Arthurs, D. J. Keating, B. W. Stringer, and S. J. Conn, "The suitability of glioblastoma cell lines as models for primary glioblastoma cell metabolism," *Cancers (Basel)*, vol. 12, no. 12, 2020, Art. no. 3722.

Supplementary Material: This article contains supplementary material (https://doi.org/10.1515/mim-2025-0031).